MECHANICS OF ADVANCED MATERIALS AND STRUCTURES

An International Journal

EDITOR-IN-CHIEF

Professor J. N. Reddy

Department of Mechanical Engineering
Texas A & M University
College Station, TX 77843-3123, USA
Tel: (979) 862-2417; fax: (979) 845-3081
e-mail: jnreddy@tamu.edu

Abstracted/indexed in: Materials Science Citation Index; and Current Contents/Engineering, Computing, and Technology; Cambride Scientific Abstracts: Aluminum Industry Abstracts; Cambridge Scientific Abstracts: Engineered Materials Extracts; Cambridge Scientific Abstracts: Metals Abstracts/METADEX; Science Citation Index Expanded.

Mechanics of Advanced Materials and Structures (ISSN: 1537-6494) is published bimontly in February, April, June, August, October, and December for a total of 6 issues per year by Taylor & Francis Group, LLC, 325 Chestnut Street, Philadelphia, PA 19106. Periodicals postage paid (Permit no. 022-723) at Philadelphia, PA and additional mailing offices.

US Postmaster: Please send address changes to *Mechanics of Advanced Materials and Structures* c/o Taylor and Francis, 325 Chestnut Street, Philadelphia, PA 19106, USA.

Annual Subscription, Volume 13, 2006
Print ISSN - 1537-6494, Online ISSN - 1537-6532
Institutional subscribers: $1068 (US) £647 (UK)
Personal subscribers: $377 (US) £228 (UK)
An institutional subscription to the print edition includes free access to the online edition for any number of concurrent users across a local area network.
Production and Advertising Office: 325 Chestnut Street, Philadelphia, PA 19106. Tel - 215-625-8900, Fax - 215-625-8563. Production Editor: Rebecca A. Corpier.
Subscription offices
USA/North America: Taylor & Francis Group, LLC, 325 Chestnut Street, Philadelphia, PA 19106. Tel: 215-625-8900, Fax: 215-625-2940.
UK/Europe: Taylor & Francis Customer Services, Sheepen Place, Colchester, Essex CO3 3LP, UK. Tel:+44-(0)-20-7017-5544, Fax:+44-(0)-20-7017-5198.

For a complete guide to Taylor & Francis Group's journal and book publishing programs, visit our website: **www.taylorandfrancis.com.**

October 2006

Mechanics of Advanced Materials and Structures, 13:443–455, 2006

ISSN: 1537-6494 print / 1537-6532 online
DOI: 10.1080/15376490600862863

Taylor & Francis
Taylor & Francis Group

Finite Element Analysis of Phase Transformation Dynamics in Shape Memory Alloys with a Consistent Landau-Ginzburg Free Energy Model

D. Roy Mahapatra and R. V. N. Melnik
Mathematical Modelling and Computational Sciences, Wilfrid Laurier University, Waterloo, ON N2L3C5, Canada

The Landau theory of phase transition has been successfully applied to solve a number of important problems in the dynamics of martensitic phase transformations in alloys. On the other hand, although a precise mathematical description of the microstructures is known within the framework of Cauchy-Born hypothesis, its discrete version is not well elucidated in the literature, especially for multivariant transformations in three-dimensional samples. A major reason for such a situation lies with computational difficulties connected with quasi-convexity of the associated minimization problem. In this paper we develop a Landau-Ginzburg free energy model for dynamic problems of phase transformations and show a possible link of the developed framework with the continuum description of phase transformations. We demonstrate how the precise description of compatible microstructures in the phase-field model can be used in computational finite element models. The developed framework is sufficiently general to be applied to different types of phase transforming alloys and under general thermo-mechanical loadings. We exemplify the developed technique and its finite element implementation on cubic to tetragonal transformations.

Keywords austenite, martensite, transformation, microstructure, free energy, finite element

1. INTRODUCTION

Shape Memory Alloys (SMAs) have a growing number of applications in transducer devices and control of dynamical systems. However, design and analysis involving new SMA structures remain to be difficult tasks. Although there are a number of phenomenological models available in the literature, each such model is typically applicable only to a specific type of problems, while practical requirements dictate the necessity to deal with a range of thermomechanical loadings for experimental characterizations. Mathematical models for SMAs can be categorized into: (a) phenomenology-based models that use the generalized framework of plasticity [1–4], (b) models based on the theory of compatible microstructures [5–8], and (c) phase-field models based on the theory of first-order phase kinetics [9–11]. The phenomenology based models have been studied widely and they have been tuned to predict the accurate dynamics for several classes of SMAs under specific loading conditions. However, these models vary drastically depending on the nature of the shape memory phenomenon that is being simulated (i.e., superelasticity, thermally induced, or combined thermo-mechanical transformations), material constants, conditions at which experiments are done, effective dimensions and shapes of the samples. In most such models, the entire domain of a single crystal or domains of polycrystals are represented by a homogenized volume fraction of phases. In a quasi-static sense, a detailed description of the transformed texture within the domains has been reported by Siredey et al. [4] and later by Niclaeys et al. [12] for multivariant interactions in three-dimensions. However, analyzing the microstructure under general dynamic loadings with such approaches requires that all the interfaces (e.g., the normal vectors to such interfaces) should be tracked as the sequence of energy minimization processes is carried out. As it stands today, this is a drawback of the modelling strategy that ultimately is a consequence of the basic building block in the phenomenological models. Indeed, when the process variables are defined, the condition for phase transformations (PT) is introduced by first separating out the dissipation energy due to phase transformations from that of the reorientation and from the energy of heat conduction. Then the phenomenology of yielding is introduced to preserve the positivity condition on the energy dissipation due to the phase transformation. This leads to the loss of convexity observed during the phase transformation and to substantial computational difficulties in the solution of the problem. In order to deal with the dynamic nature of the problem, a relaxed variational framework is required [13]. Multiple energy wells, which correspond to individual phases in the self-accommodating microstructures, lead to non-convexity. However, in a quasi-static sense, the kinematics of the self-accommodating microstructures can be described now by using the "compatibility condition" and the "twinning

Received 26 April 2006.
Address correspondence to R. V. N. Melnik, Mathematical Modelling and Computational Sciences, Wilfrid Laurier University, Waterloo, ON N2L3C5, Canada. E-mail: rmelnik@wlu.ca

condition" [6]. In this case, the rate-dependent terms in the deformation process are not directly present in such a description, and thus the usual conservation law needs to be augmented by using the phase kinetics [14]. Therefore, if the non-negativity condition of the thermodynamic dissipation potential is not imposed in a consistent way, this leads to a significant drawback of phenomenological models applied to the analysis of the effect of loading rates.

In the development of free-energy-based mesoscopic and microscopic models, Landau's theory has played a crucial role [15]. However, it is known that in three-dimensional situations such free energy models may lead to unphysical minima. Niclaeys et al. [12] have reported an approach based on a multivariant interaction potential constructed on the assumption of non-vanishing stress due to inclusions in a "cluster of variants." While this type of models uses volume averaged phase fractions, a further downscaling within the polycrystals is not reliable within this approach, and therefore one should resort to the physical description of crystallographic variants as reported by Levitas and Preston [16–18]. Typically, this is done by introducing the order parameters which are ensemble averages of the atomic order variables associated with the vibrating lattices in individual crystallographic states. The description of the evolution of microstructure then becomes possible in a sense of upwinding the physical information of solid-state phase transformations in SMA (atomic reordering rather than diffusion) which is first-order in nature. A mathematical model based on this microscopic framework has been developed by the authors of the present paper in Ref. [19] as an extension of the model reported in [16–18]. In the present paper, we report the detailed formulation of the Landau-Ginzburg free energy model and the subsequent variational framework. We discuss our computer implementation for cubic-to-tetragonal transformations and report details of numerical simulation of stress-induced and thermally induced transformation dynamics in a NiAl single crystal 3D sample.

The paper is organized as follows. In Sec. 2 we outline the steps to derive the free energy function in the case of multivariant phase transformations with essential properties of frame-indifference and material symmetry. An extension of this procedure to the three-dimensional multivariant case is given in Sec. 3. The link between the phase-field evolution and microstructural compatibility condition is discussed in Sec. 4. The behaviour of the energy wells under thermo-mechanical deformation is simulated numerically and the results are presented in Sec. 5. Nonequilibrium thermodynamics issues are discussed in Sec. 6. Finite element implementation and its variational framework are presented in Sec. 7. Numerical characterization of stress and temperature induced transformation dynamics are presented in Section 8.

2. LANDAU-GINZBURG FREE ENERGY MODEL

In what follows we aim at a consistent development of the Landau-Ginzburg free energy with minimal number of constants. Some of these constants (e.g. elastic and thermal properties of the phases, entropy jump during transformation, kinetic coefficients etc.) can be characterized by molecular dynamic simulation. The constants that influence the mechanical and thermal hysteresis loop can be characterized from experiments on single crystals. Further, the additional mechanisms, which are not modeled at present (e.g. dislocation, creep etc.), but inherent in polycrystalline samples, and which influence the transformation dynamics, can be included by tuning the latter constants (e.g. a free energy scale parameter G_0 discussed in detailed toward the end of the paper). Below, the Landau-Ginzburg theory is discussed in the context of first-order phase-field evolution applicable to SMAs (see [9–11, 15]) and in the context of its link with the microstructural compatibility [6] under the framework of macroscopic continuum deformation discussed earlier.

A major advantage of the proposed approach is that the finite element mesh adaptation based on a strong estimate (which is due to the motion of the sharp interfaces) need not be necessary as we interpolate the phase field (represented by order parameter η). However, a consistent evolution criteria need to be derived from the analytic description of the microstructure by using the compatibility conditions. Here, we outline the possible steps to achieve this.

Another important issue discussed below is how to describe the energy wells $G(\eta)$ in the case of multivariant phase transformations with essential properties of frame-indifference and material symmetry. Further conditions are to be imposed regarding uniqueness of the evolution, that only a single variant is formed at a given material point in space and time. Details of a systematic approach to impose these conditions can be found in [16, 17].

Finally, the evolution of the ordered states, or equivalently, the A-M compatible microstructure, is governed by the first-order kinetics of the time-dependent Ginzburg-Landau equation [11, 18]. The underlying step here is to obtain, on one hand, the atomistic reordering without diffusion and the resulting free energy $G(\eta)$ (or the related constants and spontaneous strain at equilibrium temperature) based on Born-Oppenheimer approximation, and on the other hand, express this free energy (equivalently $G(F)$) according to the Cauchy-Born hypothesis of lattice deformation (F). The order parameters (η) therefore describe the phenomenological link between the above two dynamics. This approach deviates from the notion of phase fractions [1, 4, 20] and gives a consistent framework for the evolution of microstructure in multivariant situations. Several preliminary results on the implementation of the above approach have been recently reported in [21]. Rigorous results on numerical procedures for the several simplified models have been reported in Li and Luskin [22], Matus et al. [23] (see also references therein). However, as one resolves the kinematics at the scales of several evolving martensitic plates, this leads to significant computational difficulty, and results related to the three-dimensional time-dependent dynamics of real-scale SMA devices are virtually absent in the literature.

It has been demonstrated by Levitas and Preston [16, 18] that the polynomial structures 2-3-4 and 2-4-6 of the Gibbs free energy in the order parameter η in Cartesian coordinates can eliminate the problem of unphysical minima and retain all the necessary properties of the Ginzburg-Landau free energy function with respect to point group symmetry of the crystals. Here the numbers (for example 2, 3 and 4 in 2-3-4) stand for the power of the order parameter (or strain invariance in other available models) in the consecutive terms of the polynomial. Also such polynomial structure can be made in such a way that the stability of the austenitic phase (A) and the martensitic variants (M_j, $j = 1, \ldots, N$), non-minimum transformation barrier and the nucleation can be described in stress-temperature space. Here N is the number of variants. Also, while using such a polynomial structure, the interfaces (domain walls) $M_j - M_i$ between the martensitic variants (i, j) can be interpreted by using a newly introduced barrierless A nucleation mechanism, i.e. by splitting the original into two simultaneously present interfaces $M_j - A$ and $A - M_i$. In this section a 2-3-4 polynomial structure is constructed systematically from the basic structure of the energy well. As a result, we arrive at (a) the amount of strain that is developed as the transformation takes place and (b) the analytical description of transformation barrier which is dependent of stress and temperature.

Let us first consider a single variant of martensite and single order parameter $\eta \in [0, 1]$. We define the Gibbs free energy density in stress-temperature space $(\boldsymbol{\sigma}, \theta)$ as

$$G(\eta) = -\boldsymbol{\sigma} : \boldsymbol{\lambda} : \boldsymbol{\sigma}/2 - \boldsymbol{\sigma} : \boldsymbol{\varepsilon}^t \varphi(\eta) + f(\theta, \eta), \qquad (1)$$

where $\boldsymbol{\lambda}$ is the constant fourth-rank elastic compliance tensor, $\boldsymbol{\varepsilon}^t$ is the transformation strain tensor at the thermodynamic equilibrium of the martensite (obtained from crystallography), $\varphi(\eta)$ is a monotonic function with $\varphi(0) = 0$ indicating stable A phase and $\varphi(1) = 1$ indicating stable M phase. $f(\theta, \eta)$ is the chemical part of the energy with property: $f(\theta, 1) - f(\theta, 0) = \Delta G^{\theta}(\theta)$, where ΔG^{θ} is the difference between the thermal parts of the Gibbs free energy density of the M and A phases, which can be obtained indirectly from experiments through the relation [24]

$$\Delta G^{\theta} = -\Delta s_e(\theta - \theta_e) - \Delta c\theta\,[\ln(\theta/\theta_e) - 1] - \Delta c\theta_e, \qquad (2)$$

where Δc is the difference between the specific heat of the phases, Δs_e is the jump in the specific entropy at the equilibrium temperature (θ_e). The objective is to obtain the functions φ and f by satisfying their properties mentioned above and the conditions of extremum of the energy for existence of equilibrium of A and M phases: $\partial G/\partial\eta = 0$ at $\eta = 0, 1$. Since there should be intermediate values of η during PT, we assume the following polynomial structure of the extremum by calling this intermediate value as the transformation barrier η^b. Thus

$$\frac{\partial G}{\partial \eta} = G_0\eta(\eta - 1)(\eta - \eta^b), \qquad (3)$$

so that the roots $\eta = 0, 1$ correspond to the extrema and the root $\eta = \eta^b(\boldsymbol{\sigma}, \theta)$ represents the $A \leftrightarrow M$ PT barrier. Here G_0 is a scaling factor which is generally independent of stress but can depend in temperature. This argument is to leave the scope to experimentally characterize G_0 based on the fact that the stress hysteresis in metals and alloys are independent of temperature. However G_0 may be used to accommodate other sources of inelasticity, such as dislocation, although this issue is not addressed in the present work.

At equilibrium, we have [19]

$$\frac{\partial G}{\partial \eta} = -\boldsymbol{\sigma} : \boldsymbol{\varepsilon}^t \frac{\partial \varphi(\eta)}{\partial \eta} + \frac{\partial f(\theta, \eta)}{\partial \eta} = 0, \quad \eta = 0, 1. \qquad (4)$$

The total strain tensor ($\boldsymbol{\varepsilon} = -\partial G/\partial\boldsymbol{\sigma}$) is the sum of the elastic strain tensor ($\boldsymbol{\lambda} : \boldsymbol{\sigma}$) and the transformation strain tensor ($\boldsymbol{\varepsilon}^t \varphi(\eta)$). Hence, for reconstructive PT through vanishing misfit strain, the condition

$$\boldsymbol{\sigma} : \boldsymbol{\varepsilon}^t \frac{\partial \varphi(\eta)}{\partial \boldsymbol{\sigma}} - \frac{f(\theta, \eta)}{\partial \boldsymbol{\sigma}} = 0 \quad \forall(\boldsymbol{\sigma}, \eta) \qquad (5)$$

must be satisfied. It is observed in the reported results [16] that the transformation barrier is dependent on stress. In the context of transformation barrier, Levitas and Preston [18] have treated the associated η as dependent on $\boldsymbol{\sigma}$ by method of trials such that all the ranges of values of the coefficient of the polynomial are self-consistent. In our model, we employ a systematic approach by considering stress-dependent barrier height because the stress $\boldsymbol{\sigma}$ is the only driving factor for PT under isothermal condition. Integrating Equation (3) and imposing the combined properties of $\varphi(\eta)$ and $f(\theta, \eta)$ stated earlier as

$$G(\boldsymbol{\sigma}, \theta, 0) - G(\boldsymbol{\sigma}, \theta, 1) = \boldsymbol{\sigma} : \boldsymbol{\varepsilon}^t - \Delta G^{\theta}, \qquad (6)$$

we get that

$$\eta^b = \frac{1}{G_0}[-6\boldsymbol{\sigma} : \boldsymbol{\varepsilon}^t + 6\Delta G^{\theta}] + \frac{1}{2}. \qquad (7)$$

Here the contribution of thermal strain has been neglected. Using Equation (1) in Equation (3) and by differentiating with respect to $\boldsymbol{\sigma}$, one has

$$-\boldsymbol{\varepsilon}^t \frac{\partial \varphi(\eta)}{\partial \eta} - \boldsymbol{\sigma} : \boldsymbol{\varepsilon}^t \frac{\partial^2 \varphi(\eta)}{\partial \boldsymbol{\sigma}\partial \eta} + \frac{\partial^2 f(\theta, \eta)}{\partial \boldsymbol{\sigma}\partial \eta} = G_0 \frac{\partial}{\partial \boldsymbol{\sigma}}[\eta^b\eta - (\eta^b + 1)\eta^2 + \eta^3]. \qquad (8)$$

The term involving f can be eliminated from Equation (8) with the help of Equation (5), and can be expressed as

$$\boldsymbol{\varepsilon}^t \frac{\partial \varphi(\eta)}{\partial \eta} = G_0\eta(\eta - 1)\frac{\partial \eta^b}{\partial \boldsymbol{\sigma}} = \eta(\eta - 1)(-6\boldsymbol{\varepsilon}^t). \qquad (9)$$

Integrating Equation (9) and following the properties of the transformation strain, i.e. $\varphi(0) = 0$ and $\varphi(1) = 1$, we get

$$\varphi(\eta) = 3\eta^2 - 2\eta^3, \quad \eta \in [0, 1]. \tag{10}$$

Substituting this form in Eq. (5) and integrating with respect to η, the chemical part of the free energy density is obtained as

$$f(\theta, \eta) = \boldsymbol{\sigma} : \boldsymbol{\varepsilon}^t(3\eta^2 - 2\eta^3) + G_0 \times \left[\frac{1}{2}\eta^b\eta^2 - \frac{1}{3}(\eta^b + 1)\eta^3 + \frac{1}{4}\eta^4\right]. \tag{11}$$

For $A \rightarrow M$ PT, the criteria for the loss of stability of A phase is $\partial^2 G/\partial\eta^2 \leq 0$ at $\eta = 0$, which gives the condition for stress-induced transformation:

$$\boldsymbol{\sigma} : \boldsymbol{\varepsilon}^t \geq \Delta G^\theta + \frac{G_0}{12}. \tag{12}$$

Similarly, for $M \rightarrow A$ PT, the criteria for the loss of stability is $\partial^2 G/\partial\eta^2 \leq 0$ at $\eta = 1$, which gives the condition for stress-induced transformation:

$$\boldsymbol{\sigma} : \boldsymbol{\varepsilon}^t \leq \Delta G^\theta - \frac{G_0}{12}. \tag{13}$$

$M_j \leftrightarrow M_i$ PT or diffused interface can evolve for stresses outside the range obtained by Eqs. (12) and (13). Note that no parameter fitting is required in the present model as opposed to the earlier model [16], except the scaling factor G_0. In the numerical simulation we use $G_0 = -0.5\Delta s_e\theta_e$. Equations (12) and (13) indicate a nonlinear dependence of the transformation surface on the temperature, which can be compared with the experimental data.

2.1. Cubic to Tetragonal Transformation Characteristics

We now consider the cubic to tetragonal PT for single variant martensitic case in absence of the elastic part of the stress. After reducing the stress and strain tensors in 1D, the equilibrium stress-transformation curve is obtained as

$$\eta = \eta^b \Rightarrow \sigma = \frac{1}{\varepsilon^t}\left[\Delta G^\theta + G_0\frac{1 - 2\eta}{12}\right]. \tag{14}$$

Note that the increase in η causes decrease in σ which is consistent. Then the stress hysteresis can be written as

$$\sigma_{(\eta=0)} - \sigma_{(\eta=1)} = \frac{G_0}{6\varepsilon^t}, \tag{15}$$

which is independent of the temperature. Equation (14) also shows nonzero tangent moduli where A and M lose their stability. These observations coincide with the results from the earlier model [16].

3. MULTIVARIANT PHASE TRANSFORMATION

In order to model realistic situations and macroscopic sample of SMA, it is essential to incorporate the effects of the following: (1) martensitic variants (M_k) (2) thermal strain (3) unequal compliances across the interfaces and the resulting inhomogeneity. In this paper we consider cubic-to-tetragonal transformations for numerical studies. In this case, there are three variants of martensite according to the point group of crystallographic symmetry. The Gibbs free energy density thus should poses the associated invariance properties. In the mathematical model, this can be cross-checked by interchanging the variant indices (k). We assume the same order of variation in the compliance tensor and the thermal expansion tensor as in $\varphi(\eta)$. The Gibbs free energy density for cubic-tetragonal transformation having three variants $k = 1, 2, 3$ is expressed as

$$\begin{aligned} G(\eta) = &-\boldsymbol{\sigma} : \left[\boldsymbol{\lambda}_0 + \sum_{k=1}^{3}(\boldsymbol{\lambda}_k - \boldsymbol{\lambda}_0)\varphi(\eta_k)\right] : \boldsymbol{\sigma}/2 \\ &-\boldsymbol{\sigma} : \sum_{k=1}^{3}\boldsymbol{\varepsilon}_k^t\varphi(\eta_k) - \boldsymbol{\sigma} : \left[\boldsymbol{\varepsilon}_{\theta 0} + \sum_{k=1}^{3}(\boldsymbol{\varepsilon}_{\theta k} - \boldsymbol{\varepsilon}_{\theta 0})\varphi(\eta_k)\right] \\ &+ \sum_{k=1}^{3} f(\theta, \eta_k) + \sum_{i=1}^{2}\sum_{j=i+1}^{3} F_{ij}(\eta_i, \eta_j), \end{aligned} \tag{16}$$

where $\boldsymbol{\lambda}$ is the second-order forth-rank compliance tensor ($\boldsymbol{\lambda}_0$ is for A phase), $\boldsymbol{\varepsilon}_{\theta 0} = \boldsymbol{\alpha}_0(\theta - \theta_e)$, $\boldsymbol{\varepsilon}_{\theta k} = \boldsymbol{\alpha}_k(\theta - \theta_e)$, $\boldsymbol{\alpha}_0$ and $\boldsymbol{\alpha}_k$ are the thermal expansion tensor of A and M_k. F_{ij} is an interaction potential required to preserve the frame-invariance of G with respect to the point group of symmetry and uniqueness of the multivariant PT at a given material point. The description of PT can now be generalized with three sets of order parameters: $\bar{0} = \{0, \eta_k = 0, 0\}$, $\bar{1} = \{0, \eta_k = 1, 0\}$ and $\bar{\eta}_k = \{0, \eta_k, 0\}$. The extremum property of the free energy density requires

$$\frac{\partial G}{\partial \eta_k} = G_0\eta_k(\eta_k - 1)\left(\eta_k - \eta_k^b\right) = 0, \quad \eta_k = \bar{0}, \bar{1}, \tag{17}$$

$$\frac{\partial^2 G}{\partial \eta_k^2} \leq 0, \quad \eta_k = \bar{0} \quad (A \rightarrow M_k) \tag{18}$$

$$\frac{\partial^2 G}{\partial \eta_k^2} \leq 0, \quad \eta_k = \bar{1} \quad (M_k \rightarrow A) \tag{19}$$

The transformation energy associated with $A \leftrightarrow M_k$ is

$$G(\boldsymbol{\sigma}, \theta, \bar{0}) - G(\boldsymbol{\sigma}, \theta, \bar{1}) = \boldsymbol{\sigma} : \boldsymbol{\varepsilon}_k^t - \Delta G^\theta. \tag{20}$$

Combining Eqs. (18) and (20) with similar steps described in Sec. 2, we get

$$\eta_k^b = \frac{1}{G_0}\big[-6\boldsymbol{\sigma} : \boldsymbol{\varepsilon}_k^t - 3\boldsymbol{\sigma} : (\boldsymbol{\lambda}_k - \boldsymbol{\lambda}_0) : \boldsymbol{\sigma} - 6\boldsymbol{\sigma} : (\boldsymbol{\varepsilon}_{\theta k} - \boldsymbol{\varepsilon}_{\theta 0}) + 6\Delta G^\theta\big] + \frac{1}{2} \tag{21}$$

Following the steps given in [17], we arrive at the frame-invariance as well as symmetry preserving polynomial structure of the interaction potential

$$F_{ij} = \eta_i\eta_j(1-\eta_i-\eta_j)[B\{(\eta_i-\eta_j)^2-\eta_i-\eta_j\}+D\eta_i\eta_j s] + \eta_i^2\eta_j^2(\eta_i Z_{ij}+\eta_j Z_{ji}) \quad (22)$$

where B, D are constants to be estimated from experiments, The transformation energy associated with $M_i \rightarrow M_j$ is already satisfied in this approach. Finally, the uniqueness of multi-variant PT at a material point is now imposed, which leads to

$$\frac{\partial}{\partial\sigma}\left[\sum_{k=1}^{N-1}\sum_{j=k+1}^{N}\frac{\partial F_{kj}(\eta_k,\eta_j)}{\partial\eta_k}\right] = \sum_{k=1}^{N}\left[\varepsilon_k^t\frac{\partial\varphi(\eta_k)}{\partial\eta_k} + (\varepsilon_{\theta k}-\varepsilon_{\theta 0})\frac{\partial\varphi(\eta_k)}{\partial\eta_k} + (\lambda_k-\lambda_0)\frac{\partial\varphi(\eta_k)}{\partial\eta_k}\sigma\right], \quad (23)$$

The constants Z_{ij} can be estimated with the help of Eq. (23). The main significance of Eq. (23) is that it governs the reorientation of the variants and interfaces and hence the relaxation of the stresses. This is to say, the formalism of stress due to inclusions in the "cluster of variants" as developed in [12] is addressed here without making the assumption that it can be decomposed as sum of the stress due to elastic deformation and due to inclusion.

It can be noted that the energy density is represented in stress-temperature space. In this way the direct use of the deformation gradient associated with the phase transformation is avoided. As a consequence, analysis in stress space without explicitly addressing the stress-strain hysteresis becomes convenient (see [17]). On the other hand, if the atomic reordering during transformation is expressed in terms of continuum deformation gradient $\boldsymbol{F} = \nabla\boldsymbol{y}(\boldsymbol{x})$, then the associated large strain for the two differently derived models can be given by

$$\frac{1}{2}(\boldsymbol{F}^T\boldsymbol{F}-\boldsymbol{I}) = -\frac{\partial G(\eta)}{\partial\sigma} = \varepsilon_{\mathrm{el}} + \sum_k \varepsilon_k^t\varphi(\eta_k), \quad (24)$$

where $\varepsilon_{\mathrm{el}}$ is the elastic part of the total strain from Eq. (16). For a compatible microstructure that minimizes $G(\boldsymbol{F}) \in \mathcal{K}$ at the austenitic well, where $\mathcal{K}$ is the sequence of energy wells, it follows from the Cauchy-Born hypothesis that

$$\hat{\mathbf{e}}^m = \boldsymbol{F}^m\boldsymbol{U}_m\boldsymbol{F}^a\hat{\mathbf{e}}^o, \quad (25)$$

where $\hat{\mathbf{e}}^m$ and $\hat{\mathbf{e}}^o$ are the lattice vectors for the mth variant of M and the undeformed A lattice vector respectively. Under zero stress, $\boldsymbol{F}^m = \boldsymbol{F}^a = \boldsymbol{R}$ is a rigid rotation. $\boldsymbol{U}_m$ is the Bain matrix or the *transformation matrix* [6]. At the onset of spontaneous transformation, we can drop the elastic strain part in Eq. (25) such that

$$\frac{1}{2}(\boldsymbol{U}_m^T\boldsymbol{U}_m-\boldsymbol{I}) = \sum_k \varepsilon_k^t\varphi(\eta_k). \quad (26)$$

ε^t can now be estimated considering stress-free martensitic plates ($\eta_k = 1$) for which $\boldsymbol{U}_m$ are known. Hence, one can write

$$\varepsilon_k^t = \frac{1}{2}(\boldsymbol{U}_m^T\boldsymbol{U}_m-\boldsymbol{I}). \quad (27)$$

Left hand side of Equation (26) is a point-wise description, whereas the right hand side requires a spatial structure $\eta_k \in \{\eta_k(\boldsymbol{x})\}$. Interestingly, this spatial description is already present in $\boldsymbol{F}(\boldsymbol{x})$, and also in certain cases, e.g. for rank-one connected phases under plane strain condition, there exists closed form solutions [5]. For 3D situation with more complex interfaces, solution can be sought numerically. A general approach that one can adopt to introduce such microstructural compatibility in the phase-field is described below.

4. COMPATIBLE MICROSTRUCTURE

Let us consider the alternate array like microstructure shown in Figure 1 often observed in micrographs of SMA, where λ is the alternate M width. The average deformation gradients in A, M_k are respectively $\boldsymbol{F}^{(o)}$, $\boldsymbol{F}^{(k)}$. For given transformation matrices $\boldsymbol{U}_k$, let λ_1, λ_2, λ_3 be the eigenvalues of $\boldsymbol{U}_k$. For the average deformation across the M_1–M_2 interfaces to be compatible (for detail derivation see [6])

$$\boldsymbol{F}^{(2)} - \boldsymbol{F}^{(1)} = \boldsymbol{a}' \otimes \hat{\mathbf{n}}. \quad (28)$$

This is called the twinning equation. For the A-M_k be formed as n increases but for an interface to exist with continuous deformation,

$$\lambda\boldsymbol{F}^{(2)} + (1-\lambda)\boldsymbol{F}^{(1)} - \boldsymbol{F}^{(o)} = \boldsymbol{b} \otimes \hat{\mathbf{m}}. \quad (29)$$

a' and b are some scaler to be identified. This is called the A-M interface equation. Using the invariance properties, i.e.,

$$\boldsymbol{F}^{(o)} = \boldsymbol{I}, \quad \boldsymbol{F}^{(1)} = \boldsymbol{Q}_1\boldsymbol{U}_1, \quad \boldsymbol{F}^{(2)} = \boldsymbol{Q}_2\boldsymbol{U}_2 \quad (30)$$

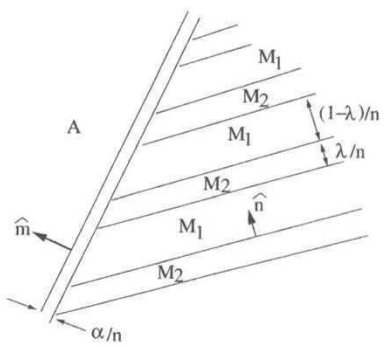

FIG. 1. Alternate array of microstructure originating from austenite wall.

and so on for all the variants, where $\boldsymbol{Q}$ is some rotation matrix, one finds

$$\boldsymbol{b} = \rho'\left(\sqrt{\frac{\lambda_3(1-\lambda_1)}{\lambda_3-\lambda_1}}\hat{\mathbf{e}}_1 \pm \sqrt{\frac{\lambda_1(\lambda_3-1)}{\lambda_3-\lambda_1}}\hat{\mathbf{e}}_2\right), \tag{31}$$

$$\hat{\mathbf{m}} = \frac{\sqrt{\lambda_3}-\sqrt{\lambda_1}}{\rho'\sqrt{\lambda_3-\lambda_1}}(-\sqrt{1-\lambda_1}\hat{\mathbf{e}}_1 \pm \sqrt{\lambda_3-1}\hat{\mathbf{e}}_2), \tag{32}$$

with $\lambda_1 \leq \lambda_2 \leq \lambda_3$ as three eigenvalues of $\boldsymbol{U}_k$, $\lambda_2 = 1$, and ρ' is such that $|\hat{\mathbf{m}}| = 1$.

For given $\boldsymbol{Q}_k$ and $\hat{\mathbf{n}}$ (the orientation of the domain walls), $\boldsymbol{F}^{(k)}$ can be solved using Equations (28) and (29). It is then reasonable to decompose Equation (26) with the variant-wise contribution of strain as

$$\frac{1}{2}\left(\boldsymbol{F}_k^T\boldsymbol{F}_k - \boldsymbol{I}\right) = \varepsilon_k^t\varphi(\eta_k). \tag{33}$$

η_k can be obtained from Equation (33) as trial solution for microstructural evolution in the proposed phase-field model. In this paper the discrete version of the minimization problem is developed based on finite element model with $\eta_k(\boldsymbol{x})$ as additional interpolation variable.

5. ENERGY WELLS UNDER THERMOMECHANICAL LOADING

For numerical illustration of the Gibbs free energy function derived in Sec. 3, we consider NiAl with two martensitic variants. Equal deviation of critical temperature from equilibrium temperature is assumed. The internal energy is assumed to be proportional to the difference between temperature and the equilibrium temperature in the close neighborhood of the transformation [17]. Figures 2(a)–(b) and 3(a) show the structure of the energy well, where the martensitic minimum can be formed at $\theta < \theta_c$ where θ_c is the critical temperature or at increasing deformation under controlled temperature. Figure 3(b) shows that the inversion-symmetry of the energy well in strain space is preserved but the axis of symmetry shifts to lower elastic deformation when the martensitic phase is formed. Results for two variants of M in rank-1 connected system are shown in Figures 4(a) and (b). It can be seen from Figures 4(a) and (b) that the free energy model retains the symmetry, invariance and uniqueness properties while accommodating the combined effect of deformation and temperature.

6. NONEQUILIBRIUM THERMODYNAMICS

It is now obvious that the order parameters $\eta_k, k = 1, \ldots, N$ should be treated as internal variables in the weak form. Also it should be noted that a jump in the free energy ΔG^θ has been introduced. The consequence of this jump as well as the jump in the strain across the $A - M_j$ interface is the thermodynamic force as a source of dissipation. The forcing term would eventually be balanced by the kinetic force. Thus, we have to establish a link between the evolution of PT and the non-negativity of the thermodynamic potential, namely the Helmholtz free energy. This is unlike the notion in plasticity-based framework (see e.g. [1, 2, 4]), where the non-negativity of the rate of phase fraction is directly enforced. In the context of our kinetic model, the variational formulation reported in [14] shows that the nonequilibrium thermodynamics leads to the time-dependent Ginzburg-Landau phase kinetics. In the present model this is derived by balancing the thermodynamic force with the kinetic force as

$$C\frac{\partial \eta_k}{\partial t} + \frac{\partial G'}{\partial \eta_k} = 0, \tag{34}$$

where C is a constant and G' is the modified Gibbs free energy including the gradient terms to account for the nonlocal nature of

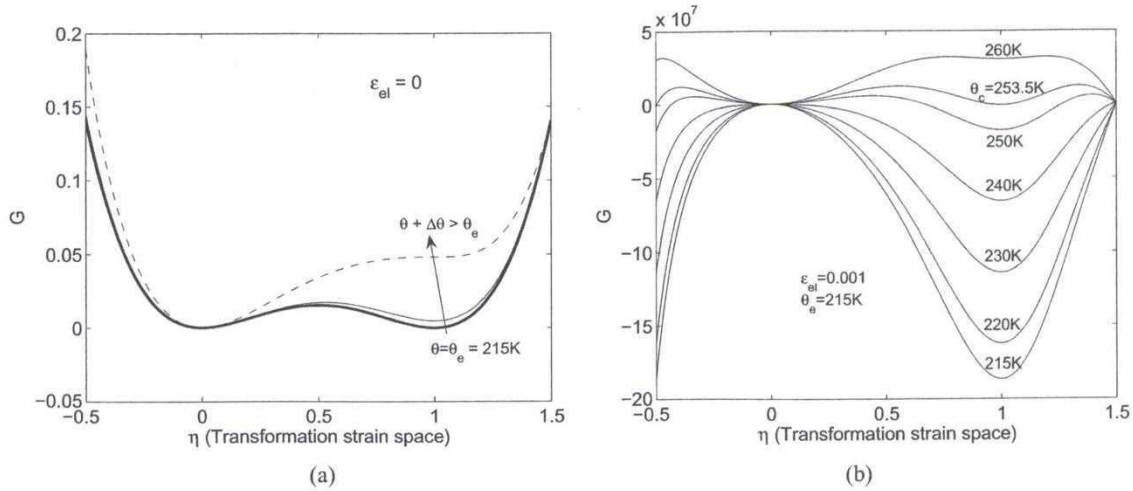

FIG. 2. (a) Austenitic well at temperature above critical temperature ($\theta_c = \theta_e$) under zero elastic deformation (b) Formation of martensitic wells at decreasing temperature and constant elastic deformation. Here $\eta = \eta_1$.

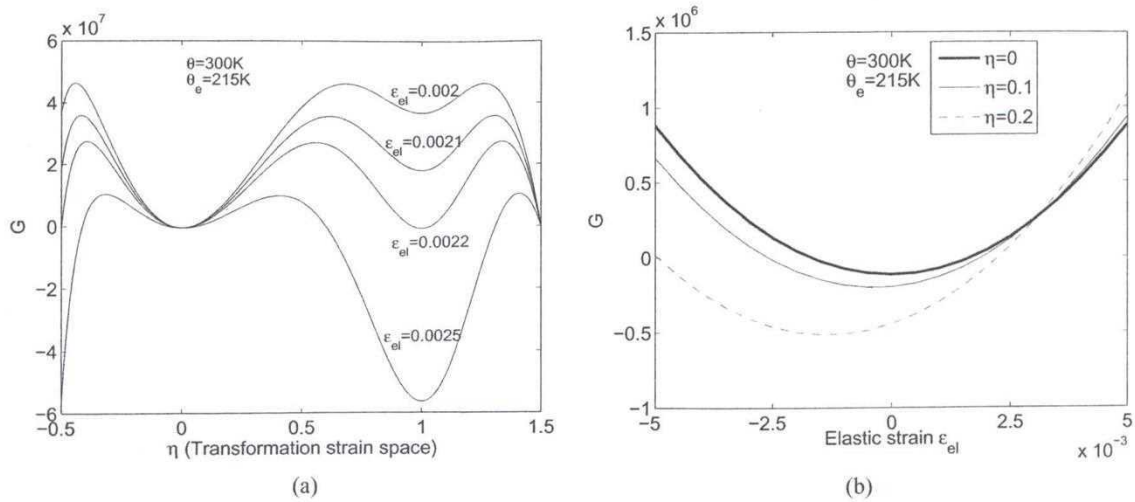

FIG. 3. (a) Formation of martensitic wells under increasing deformation and constant temperature (b) Inversion-symmetry preserving structure of the energy well during the evolution of $\eta = \eta_1$.

the interface energy. The displacements are related to the strain ε via the standard strain-displacement relation, while the stress is given by

$$\sigma = \left[\lambda_0 + \sum_{k=1}^{N}(\lambda_k - \lambda_0)\varphi(\eta_k)\right]^{-1}\left[\varepsilon - \sum_{k=1}^{N}\varepsilon_k'\varphi(\eta_k) - \varepsilon_{\theta 0} - \sum_{k=1}^{N}(\varepsilon_{\theta k} - \varepsilon_{\theta 0})\varphi(\eta_k)\right]. \tag{35}$$

In the present analysis the Green-Lagrange strain is reduced to its linear form. The phase transformation kinetics is governed by the Ginzburg-Landau equation

$$\frac{\partial \eta_k}{\partial t} = -\sum_{p=1}^{N} L_{kp}\left[\frac{\partial G}{\partial \eta_p} + \beta_p : \nabla\nabla\eta_p\right] + \theta_k, \tag{36}$$

where L_{kp} are positive definite kinetic coefficients, β_p are positive definite second rank tensor. θ_k is the thermal fluctuation satisfying the dissipation-fluctuation theorem arising in context of non-equilibrium thermodynamics. Equation (36) is complemented by the macroscopic energy conservation law

$$\frac{\partial}{\partial t}\left[\mathcal{W} - \theta\frac{\partial \mathcal{W}}{\partial \theta}\right] - \nabla\cdot(\sigma\cdot\dot{\boldsymbol{u}} - \boldsymbol{q}) = h_\theta, \tag{37}$$

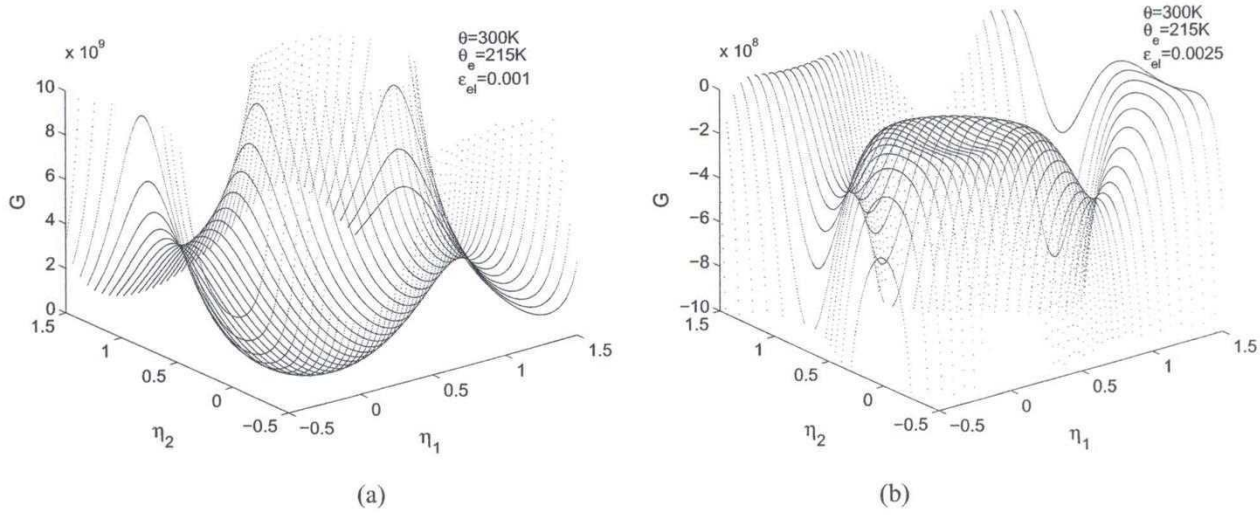

FIG. 4. (a) Unique minimum at the austenitic well ($\eta_1 = \eta_2 = 0$) under constant average deformation and temperature above the critical temperature (b) Unique martensitic wells ($\eta_1 = 1, \eta_2 = 0$) and ($\eta_1 = 0, \eta_2 = 1$) at temperature above the equilibrium temperature but under increased deformation.

and the momentum balance equation

$$\rho\frac{\partial^2 \boldsymbol{u}}{\partial t^2} = \nabla\cdot\sigma + \boldsymbol{p}, \tag{38}$$

where $\mathcal{W}$ is the Helmholtz free energy given by

$$\mathcal{W} = G + c_v\theta + \frac{1}{2}\sigma : \left[\lambda_0 + \sum_{k=1}^{N}(\lambda_k - \lambda_0)\varphi(\eta_k)\right] : \sigma + \sigma : \left[\varepsilon_{\theta 0} + \sum_{k=1}^{N}(\varepsilon_{\theta k} - \varepsilon_{\theta 0})\varphi(\eta_k)\right], \tag{39}$$

and

$$\boldsymbol{q} = -\kappa\nabla\theta - \alpha'\kappa\nabla\frac{\partial\theta}{\partial t} \tag{40}$$

is the heat flux approximated from the solution of the 3D Cattaneo-Vernotte equation, h_θ and $\boldsymbol{p}$ are the thermal loading and body force, respectively.

7. VARIATIONAL FRAMEWORK

We interpolate the fields $\boldsymbol{u}(x, y, z, t)$, $\theta(x, y, z, t)$ and $\eta_k(x, y, z, t)$ over the domain of interest, denoted by $\Omega(x, y, z) \in R^3$, using non-conforming finite elements with h-refinement. In the context of SMA, a similar scheme has been applied previously in [22]. Having the highest order of spatial derivatives in the governing equations as two, we choose the standard Lagrangian isoparametric interpolation function $\boldsymbol{N}$,

$$\{u_1 u_2 u_3\}^T = \boldsymbol{N}_u \boldsymbol{v}^e, \quad \theta = \boldsymbol{N}_\theta \boldsymbol{v}^e, \quad \eta = \boldsymbol{N}_\eta \boldsymbol{v}^e, \tag{41}$$

$$\boldsymbol{v} = \{u_1 u_2 u_3 \theta \eta_1, \ldots, \eta_n\}^T. \tag{42}$$

Here, the superscript e indicates element nodal quantities. Introducing admissible weights $\{\bar{u}_i, \bar{\theta}, \bar{\eta}_k\} \in H^{1,2}$ chosen from the linear span of $\boldsymbol{v}^e$, the variational formulation of the problem can be stated as follows

$$\delta\Pi = \delta\Pi_{PT} + \delta\Pi_\theta + \delta\Pi_u + \delta W = 0, \quad t \in [0, +\infty] \tag{43}$$

where

$$\delta\Pi_{PT} = \int_\Omega \sum_{k=1}^{N}\delta\bar{\eta}_k\left[\frac{\partial\eta_k}{\partial t} - \theta_k\right]d\mathbf{x} + \int_\Omega \sum_{k=1}^{N}\sum_{p=1}^{N}\delta\bar{\eta}_k\left[L_{kp}\left(\frac{\partial G}{\partial\eta_p} + \beta_p : \nabla\nabla\eta_p\right)\right]d\mathbf{x} - \int_\Gamma \sum_{k=1}^{N}\sum_{p=1}^{N}\delta\bar{\eta}_k L_{kp}\frac{\partial G}{\partial\eta_k}ds(\mathbf{x}), \tag{44}$$

$$\delta\Pi_\theta = \int_\Omega \delta\bar{\theta}\left[\frac{\partial}{\partial t}\left(\mathcal{W} - \theta\frac{\partial\mathcal{W}}{\partial\theta}\right) - \nabla\cdot(\sigma\cdot\dot{\boldsymbol{u}})\right]d\mathbf{x} + \int_\Omega \delta\bar{\theta}\left[\nabla\cdot\left(-\kappa\nabla\theta - \alpha'\kappa\nabla\frac{\partial\theta}{\partial t}\right)\right]d\mathbf{x} - \int_{\Gamma_\theta}\delta\bar{\theta}\boldsymbol{q}_\perp ds(\mathbf{x}), \tag{45}$$

$$\delta\Pi_u = \int_\Omega \delta\bar{\boldsymbol{u}}^T\left[\rho\frac{\partial^2\boldsymbol{u}}{\partial t^2} - \nabla\cdot\sigma\right]d\mathbf{x} - \int_\Gamma \delta\bar{\boldsymbol{u}}^T\sigma_\perp ds(\mathbf{x}), \tag{46}$$

and W is the external work done over the sample. Integrating Eqs. (43)–(46) by parts and applying divergence theorem, we obtain the discrete Euler-Lagrange form for the nonlinear finite element model, which can be expressed in matrix notations as

$$\{\delta\boldsymbol{u}\}^e: \quad \int_\Omega [\boldsymbol{N}_u]^T\rho[\boldsymbol{N}_u]\{\ddot{\boldsymbol{v}}\}^e + \int_\Omega [\boldsymbol{B}_u]^T\{\sigma\} = \int_\Gamma [\boldsymbol{N}_u]^T\{\boldsymbol{p}\} + \{\boldsymbol{f}\}^e, \tag{47}$$

$$\{\delta\theta\}^e: \quad \int_\Omega [\boldsymbol{N}_\theta]^T\rho[\dot{\boldsymbol{G}}']\{\boldsymbol{v}\}^e + \int_\Omega [\boldsymbol{N}_\theta]^T\rho[\boldsymbol{G}']\{\dot{\boldsymbol{v}}\}^e - \int_\Omega [\boldsymbol{N}_\theta]^T\rho[\boldsymbol{N}_\theta]\{\boldsymbol{v}\}^e([\nabla_\theta\dot{\boldsymbol{G}}']\{\boldsymbol{v}\}^e + [\nabla_\theta\boldsymbol{G}']\{\dot{\boldsymbol{v}}\}^e) + \int_\Omega [\boldsymbol{N}_\theta]^T\{\sigma\}^T[\nabla\boldsymbol{N}_u]\{\boldsymbol{v}\}^e + \int_\Omega [\boldsymbol{B}_\theta]^T\kappa[\boldsymbol{B}_\theta]\{\boldsymbol{v}\}^e + \int_\Omega [\boldsymbol{B}_\theta]^T\alpha'\kappa[\boldsymbol{B}_\theta]\{\dot{\boldsymbol{v}}\}^e = \int_\Gamma [\boldsymbol{N}_\theta]^T\{\boldsymbol{q}_\theta\}^e, \tag{48}$$

$$\{\delta\beta\}: \quad \int_\Omega [\boldsymbol{N}_\eta]^T[\boldsymbol{N}_\eta]\{\dot{\boldsymbol{v}}\}^e + \int_\Omega [\boldsymbol{N}_\eta]^T[\boldsymbol{L}][\boldsymbol{G}'']\{\boldsymbol{v}\}^e - \int_\Omega [\nabla\boldsymbol{N}_\eta]^T[\boldsymbol{L}][\beta][\nabla\boldsymbol{N}_\eta]\{\boldsymbol{v}\}^e + \int_\Gamma [\boldsymbol{N}_\eta]^T[\boldsymbol{L}][\beta][\nabla\boldsymbol{N}_\eta]\{\boldsymbol{v}\}^e = \int_\Gamma [\boldsymbol{N}_\eta]^T\{\theta_k\}^e, \tag{49}$$

where $[\boldsymbol{B}_u]$ is the strain-displacement matrix and $[\boldsymbol{B}_\theta]$ is its thermal analog. The stress vector is expressed as

$$\{\sigma\} = [\boldsymbol{C}(\eta_k)][\boldsymbol{B}_u]\{\boldsymbol{v}\}^e - \left[\boldsymbol{C}^t(\eta_k, \varepsilon_k^t)\right][\boldsymbol{N}_\eta]\{\boldsymbol{v}\}^e - [\boldsymbol{C}^\alpha(\eta_k, \alpha_0, \alpha_k)][\boldsymbol{N}_\theta]\left(\{\boldsymbol{v}\}^e - [\boldsymbol{I}]\{\theta_e\}\right), \tag{50}$$

where the elastic stiffness includes the phase inhomogeneity

$$[\boldsymbol{C}(\eta_k)] = \left[[\lambda_0] + \sum_k([\lambda_k] - [\lambda_0])\,\varphi(\eta_k)\right]^{-1}, \tag{51}$$

the transformation-induced stress coefficient matrix is defined as

$$\left[\boldsymbol{C}^t(\eta_k, \varepsilon_k^t)\right] = [\boldsymbol{C}(\eta_k)]\sum_k\left\{\varepsilon_k^t\right\}\bar{\varphi}(\eta_k), \tag{52}$$

$$\bar{\varphi}_k = (\varphi_k/\eta_k, 0) \quad |\eta_k| \geq 0, \tag{53}$$

and the temperature-induced stress coefficient matrix includes the phase inhomogeneity

$$[\boldsymbol{C}^\alpha(\eta_k, \alpha_0, \alpha_k)] = [\boldsymbol{C}(\eta_k)]([\alpha_0] + \sum_k([\alpha_k] - [\alpha_0])\varphi(\eta_k)). \tag{54}$$

The nonlinear terms are decomposed as

$$G = \sum_k (\bar{G}_k + \bar{F}_k)\eta_k = ([\bar{G}] + [\bar{F}])[N_\eta]\{v\}^e$$
$$= [G']\{v\}^e, \tag{55}$$
$$\left\{\frac{\partial G}{\eta_p}\right\} = [\tilde{G}]\{\eta\} = [G'']\{v\}^e. \tag{56}$$

In Equation (47), $\{f\}^e$ is the nodal force vector. In Eq. (48), $\{q_\theta\}^e$ is the thermal flux vector. Considering the effect of ambient environment surrounding the SMA sample, the total thermal flux normal to the material surface (Γ) is defined as $q_\theta = q_0 - h_c(\theta - \theta_0)$, where q_0 is the externally applied flux, θ_0 is the ambient temperature and h_c is the associated convection coefficient.

7.1. Computational Scheme

We have implemented the finite element model formalized by Equations (47)–(50) with the associated general boundary and initial conditions in a general three-dimensional finite element code. In what follows we concentrate on cubic to tetragonal transformations where we have to deal with three different phases so that $N = 3$. We employ 8-node, 7 d.o.f/node tetrahedral element with tri-linear isoparametric interpolation and reduced Gauss-quadrature integration for shear terms. For the time integration, Newmark's scheme is employed. The analysis of stability of the resulting scheme is not trivial. Here, we note only that in the context of visco-plasticity such issues were addressed in [25] for a first-order accurate integrator. Since solid-solid phase transformations involve rates that vary over a wide range, an extension of such analysis to higher-order schemes is desirable.

Since the energy minimization process can take a different and unphysical path, a special care should be taken in organizing nonlinear iterations. In particular, the phase transformation conditions in Eqs. (19)–(19) need to be enforced in a consistent manner in the incremental algorithm. The implemented algorithm can be presented in the following schematic manner:

1. With the known matrices and vectors obtained from the time step $t = t_i$, compute the stress and and transformation barrier.
2. Check the loss of stability $A \leftrightarrow M_k \; \forall k$. Obtain the increment $\Delta\eta_k$ by satisfying consistency condition in the neighborhood of the transformation surface (similar to the return mapping algorithm for elasto-plasticity [25]).
3. Compute the consistent tangent matrix $[\boldsymbol{K}]_t$. Here the effective internal force vector has three parts:

$$\{\boldsymbol{b}\} = \left\{\{f\}_u^T \{f\}_\theta^T \{f\}_\eta^T\right\}^T,$$
$$f_u = \frac{\partial \Pi_u}{\partial \boldsymbol{u}}, \quad f_\theta = \frac{\partial \Pi_\theta}{\partial \theta}, \quad f_\eta = \frac{\partial \Pi_{PT}}{\partial \eta_k}.$$

The incremental update at nth iteration is obtained as

$$\{\Delta v\}_{n+1}^e = -[\boldsymbol{K}]_t^{-1}\left(\{\boldsymbol{b}\}_{n+1}^{\text{int}} - \{\boldsymbol{b}\}_{n+1}^{\text{ext}}\right), \tag{57}$$
$$[\boldsymbol{K}]_t = \bigcup_e \frac{\partial \boldsymbol{b}}{\partial \boldsymbol{v}^e},$$

4. Solve Equation (58) by Newton iterations until a specified convergence is achieved.
5. Compute the updated vectors, velocity and acceleration and move to the next time step $t_{i+1} = t_i + \Delta t$.

8. NUMERICAL EXPERIMENTS

For numerical simulation we consider a 0.01 m × 0.005 m × 100 μm $Ni_{36\%wt.}$-Al film. Following boundary conditions are assumed at the edge $x = 0$: $u(0,t) = 0$, $\theta(0,t) = \theta_0$. Single crystal domain is assumed with initial state as austenite, i.e. $\eta = 0 \forall (x,y,z), t = 0$. It may be noted that the complexity of the numerics becomes enormous with all the variables and phases active. For simplicity, we restrict our simulation to an effective two-dimensional domain where we allow evolution of the two variants η_1 and η_2. Although there is a volume change affecting the change in thickness (in z direction), however, we assume $\eta_3 = 0$ everywhere. The surfaces are assumed to be in ambient environment with temperature θ_0. In all the following numerical studies we assume $\theta_e = 215K$ and the following elastic and thermal properties of NiAl: mass density $\rho = 7000.3$ kg/m^3; elastic stiffness components for austenite $C_{11} = C_{22} = C_{33} = 217.5$ GPa, $C_{12} = C_{13} = C_{23} = 161.6$ GPa, $C_{44} = C_{55} = C_{66} = (C_{11} - C_{12})/2$; elastic stiffness components for martensite $C_{11} = 453.8$ GPa, $C_{22} = C_{33} = 744.9$ GPa, $C_{12} = C_{13} = 396.7$ GPa, $C_{23} = 344.5$ GPa, $C_{44} = (C_{11} - C_{12})/2$, $C_{55} = (C_{11} - C_{13})/2$, $C_{66} = (C_{11} - C_{23})/2$; coefficients of thermal expansion $\alpha_0 = 20 \times 10^{-6}$ K^{-1}, $\alpha_1 = \alpha_2 = \alpha_3 = 18 \times 10^{-6}$ K^{-1}; thermal conductivity $\kappa = 50$ W/m-K, relaxation coefficient $\alpha' = 0$; kinetic coefficients $L_{ii} \approx \dot{\eta}_{\max}/G_0 = 0.25 \times 10^{-4}$ and $L_{ij} = 0$ for all $i \neq j$; gradient parameter $\beta_{ii} = 2.588 \times 10^{-10}$ and $\beta_{ij} = 0$ for all $i \neq j$; specific heat $c_v = 0.5$ J/gC; transformation properties $\Delta G^\theta = A_0(\theta - \theta_e)/3$, $A_0 = 4.4 \times 10^5$ N/m^2; lattice constants $a/a_0 = 0.9392$, $c/a_0 = 1.1302$. It may be noted that G_0 is a parameter which should be estimated based on the experimentally measured hysteresis for a given loading rate. Also, additional inelastic effects such as those due to grain boundary, dislocation etc. need to be characterized through functional dependence of various additional quantities (not included in the present model) to the energy scaling parameter G_0. From Equation (15), it is clear that the work density associated with hysteresis is proportional to G_0. In the following numerical simulations, we assume small hysteresis in pure single crystal with $G_0 = 0.1A_0$.

8.1. Stress Induced Transformation

Stress-induced transformation is simulated under the longitudinal harmonic stress applied at one edge $x = 0.01$ m along x. Loading frequency is kept at 5 Hz. First, the load amplitude

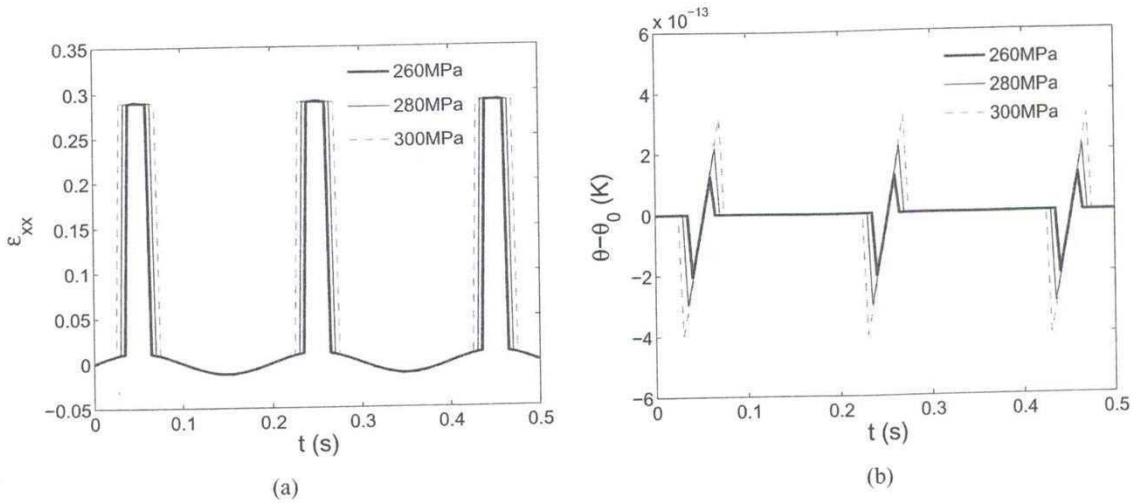

FIG. 5. (a) Strain responses and (b) thermal fluctuations at various amplitudes of the harmonic mechanical loading at $\theta_0 = 298K$.

is varied under constant $\theta_0 = 298$ K. Figure 5(a) shows the strain response due to various loading amplitudes. Here the forward and the reverse transformations can be seen at the region of sharp jumps in the strain responses. Corresponding thermal fluctuations, which are many orders of magnitude smaller than θ_0, are shown in Figure 5(b). This is well observed features of stress-induced transformation although the thermomechanical coupling and nonlinearity is inherent in the model and is not felt in these figures. It can also be noted from Figure 5 that increase in the load amplitude expands the regions of martensitic states over periodic time intervals, whereas the transformation strain remains of the same order. The change in the elastic part of the strain is not visible in the scale shown. The characteristic transformation stress for each of the three load cases are given in Table 1. It is clear from this table and from our detailed analysis that the hysteresis is independent of the stress loading amplitude or the rate of loading. This is also in agreement with the hysteresis condition derived in Eq. (15). Also, this prediction is similar to those observed in well-prepared samples of small size and with limited number of domain walls. Next, we apply the 260 MPa loading at various θ_0. The spatial distribution of the strain response and the thermal fluctuations are respectively shown in Figures 6(a) and (b). The transformation stresses for these cases are given in Table 2. It can be seen here that decrease in temperature significantly expand the martensitic state over time. Also these expanded martensitic states allow higher elastic strains. From Table 2 it can be observed that at lower values of θ_0, martensites are formed with lower transformation stress. Most importantly, these numerical simulations clearly show the influence of loading state and reference temperature on the formation of martensites.

8.2. Temperature Induced Transformation

Thermally-induced transformation is simulated under the flux q_x applied at the surface normal at $x = 0.01$ m. applied at one

TABLE 1
Transformation stresses (σ_{xx}) for the stress controlled test at $\theta_0 = 298$ K. Dimensions are in MPa

Load amplitude	A→M$_1$ start	A→M$_1$ finish	M$_1$→A start	M$_1$→A finish
260	231.64	247.26	247.30	231.70
280	226.49	249.45	249.53	226.59
300	212.10	242.67	242.77	212.23

TABLE 2
Transformation stresses (σ_{xx}) for the stress controlled test with loading amplitude of 260 M Pa. Dimensions are in MPa

θ_0	A→M$_1$ start	A→M$_1$ finish	M$_1$→A start	M$_1$→A finish
290 K	210.32	231.64	231.70	210.40
260 K	118.01	152.79	152.92	118.15
230 K	40.66	80.22	80.47	40.82

TABLE 3
Transformation temperatures θ (shown in K) for the thermal flux controlled test with flux amplitude q (shown in W/m^2)

q	A→M$_1$ start	A→M$_1$ finish	M$_1$→A start	M$_1$→A finish
4×10^7	232.00	223.73	223.62	231.95
6×10^7	234.32	217.78	217.65	234.05

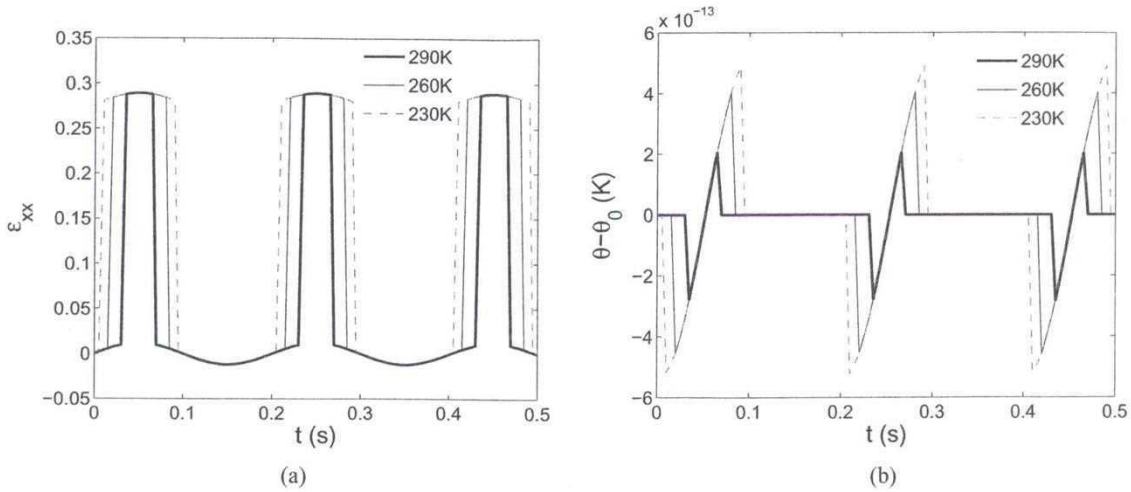

(a) (b)

FIG. 6. (a) Strain responses and (b) thermal fluctuations at various ambient temperatures θ_0 under harmonic loading amplitude of 260 MPa.

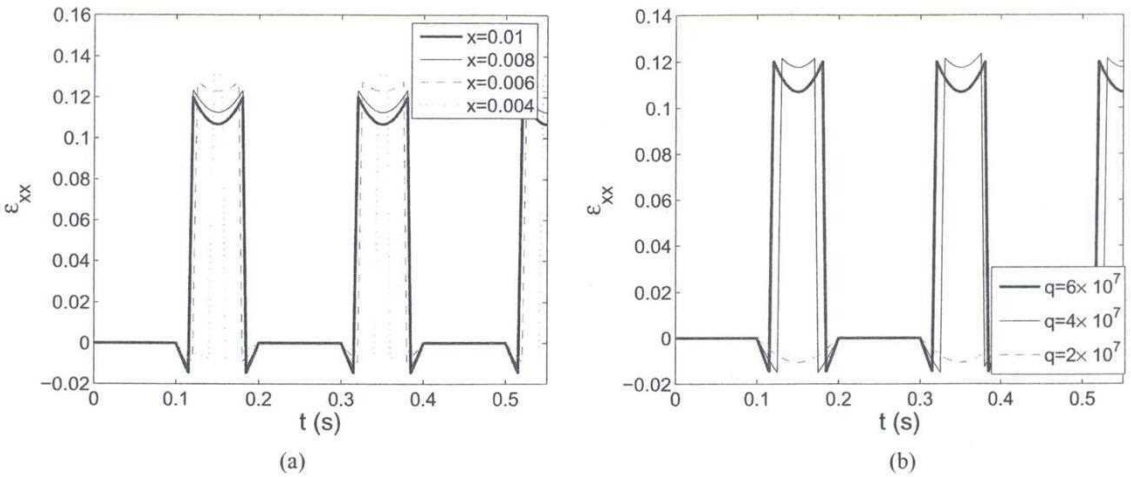

(a) (b)

FIG. 7. (a) Spatial distribution of strain response due to periodic thermal flux at $\theta_0 = 290K$ (b) strain responses due to periodic thermal flux at various q.

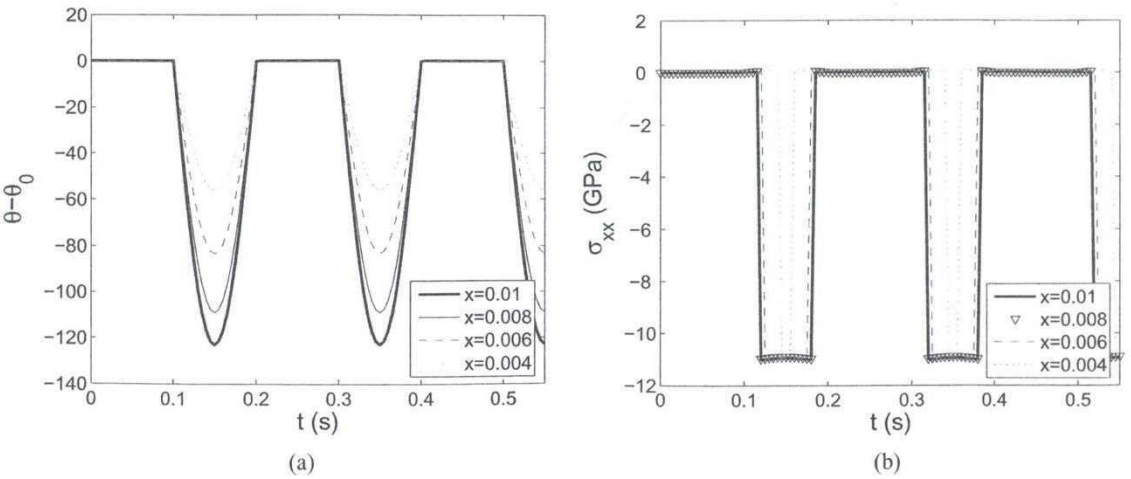

(a) (b)

FIG. 8. Spatial distributions of (a) temperature response and (b) intrinsic stress due to periodic thermal flux at $\theta_0 = 290K$.

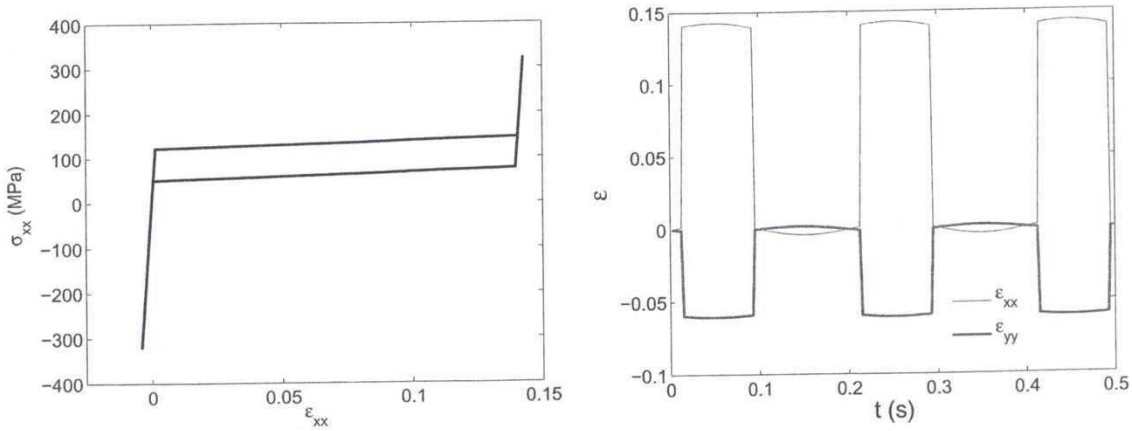

FIG. 9. (a) Mechanical hysteresis and (b) component of strains due to periodic stress at $\theta_0 = 300\ K$.

edge $x = 0.01$ m along x. Loading frequency is kept at 5 Hz. The loading history is prepared by truncating the positive (inflow) part of the harmonic flux history. This is to ensure formation of low-temperature martensites. Figure 7(a) shows the strain response at various locations due to $q = 6\times 10^7$ W/m^2, $\theta = 290$ K. Figure 7(b) shows the strain responses under various loading amplitudes. Corresponding transformation temperatures are shown in Table 3. The temperature profile and the stress profile for $q = 6 \times 10^7$ W/m^2 are respectively shown in Figures 8(a) and (b). From these results it can be seen that the increase in flux expands the martensitic states in times but in a non-proportional manner.

In the above analysis which gives a quantitative performance of the free energy model, it may be noted that for both the stress as well as the temperature induced transformations, the hysteresis is small (see Tables 1–3). It is well known that the amount of hysteresis can vary from sample to sample depending upon the method of preparation, size and constraints induced by surfaces and domain walls. The reason for small hysteresis in the above numerical tests are due to the choice of the free energy parameter G_0 which was taken as $G_0 = 0.1A_0$. In the simulations discussed next, we consider a larger value of $G_0 = 100A_0$ which is expected to produce hysteresis curves for Ni-Al as observed in experiments of macroscopic samples. Geometry and material properties are identical to those employed in previous tests. First, we show the results of isothermal loading at $\theta_0 = 300$ K. The mechanical hysteresis curve is shown in Figure 9(a) and the time histories of ε_{xx} and ε_{yy} are shown in Figure 9(b). The negative lateral strain ε_{yy} shown here for the martensitic state is according to the rotation of the lattice vectors. Here, we have used the following values for the transformation strain tensor ε_k^t: $\mathrm{Tr}(\varepsilon_k^t) = \gamma + 2\psi$, $\gamma = 0.1387$, $\psi = -0.059$. Next, a case of combined thermomechanical loading is shown in Figures 10. The applied harmonic stress and the applied harmonic flux at

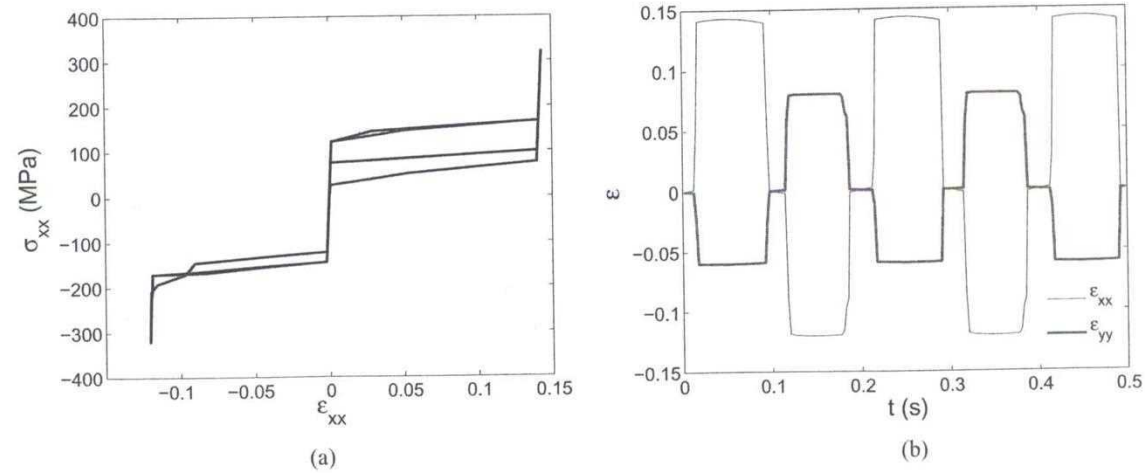

FIG. 10. (a) Mechanical hysteresis and (b) component of strains due to periodic stress and thermal flux at $\theta_0 = 300\ K$.

the end $x = 0.0$ m have the same angular phase; that is the half-cycle of tensile stress is complemented by half-cycle of heat flux in-flow. The resulting two-way shape memory effect is shown by the mechanical hysteresis curve in Figure 10(a) and the component of strains are shown in Figure 10(b). These results are indicative of a satisfactory performance of the model.

9. CONCLUSIONS

A new Landau-Ginzburg free energy model for multivariant martensitic phase transformation has been reported. It is shown that at the onset of transformation, the phase field can be uniquely identified from the conditions of microstructural compatibility. While doing so, the main advantage in the context of solving a discrete version of the energy minimization problem is that the finite element mesh needs not be adapted by tracking the A-M_k or M_k–M_j interfaces. Instead, the order parameters (η_k) can be updated from the equivalent deformation gradient in a point-wise sense. The proposed free energy model follows the essential properties of frame-invariance and material symmetry in 3D situations under different patterns of thermo-mechanical loadings. Based on the developed computational scheme, several computational results have been reported in this paper. Stress-induced transformation results are reported in this paper. Such stress-induced transformation dynamics is common in various applications of SMA actuators. Based on the proposed model and computational scheme, several possibilities in complex design optimization of SMA actuators can be explored which is an open areas of research.

REFERENCES

1. Boyd, J. G., and Lagoudas, D. C., "A thermodynamical constitutive constitutive model for shape memory materials. Part I. the monolithic shape memory alloy," *Int. J. Plasticity* **12**(6), 805–842 (1996).
2. Goo, R. C., and Lexcellent, C., "Micromechanics-based modeling of two-way memory effect of a single crystalline shape-memory alloy," *Acta Mater.* **45**, 727–737 (1997).
3. Brocca, M., Brinson, L. C., and Bazant, Z. P., "Three-dimensional constitutive shape memory alloys based on microplane model," *J. Mech. Phys. Solids* **50**, 1051–1077 (2002).
4. Siredey, N., Patoor, E., Bervellier, M., and Aberhardt, E., "Constitutive equations for polycrystalline thermoelastic shape memory alloys. Part I. Intragranular interactions and behavior of the grain," *Int. J. Solids Struct.* **36**, 4289–4315 (1999).
5. Ball, J. M., and Cartensen, C., "Compatibility conditions for microstructures and the austenite-martensite transition," *Mater. Sci. Engng. A* **273**, 231–236 (1999).
6. Bhattacharya, K., *Microstructure of Martensite*, Oxford University Press (2003).
7. James, R. D., and Hane, K. F., "Martensitic transformations and shape memory materials," *Acta Materialia* **48**, 197–222 (2000).
8. Zhu, J. J., and Lew, K. M., "Describing the Morphology of 2H Martensite Using Group Theory Part 1: Theory," *Mech. Advanced Mater. Struct.* **11**(3), 197–225 (2004).
9. Abeyaratne, R., Chu, C., and James, R. D., "Kinetics of materials with wiggly energies: The evolution of twinning microstructure in a Cu-Al-Ni shape memory alloys," *Phil. Mag.* **73A**, 457–496 (1996).
10. Artemev, A., Wang, Y., Khachaturyan, A. G., "Three-dimensional phase field model and simulation of martensitic transformation in multilayer systems under applied stresses," *Acta Mater.* **48**, 2503–2518 (2000).
11. Ichitsubo, T., Tanaka, K., Koiwa, M., and Yamazaki, Y., "Kinetics of cubic to tetragonal transformation under external field by the time-dependent Ginzburg-Landau approach," *Phy. Rev. B* **62**, 5435 (2000).
12. Niclaeys, C., Zineb, T. B., Chirani, S. A., and Patoor, E., "Determination of the interaction energy in the martensitic state," *Int. J. Plasticity*, **18**, 1619–1647 (2002).
13. Carstensen, C., "Ten remarks on nonconvex minimization for phase transition simulations," *Comput. Methods. Appl. Mech. Engng.* **194**, 169–193 (2005).
14. Ván, P., "The Ginzburg-Landau equation as a consequence of the second law," *Continuum Mech. Thermodyn.* **17**, 165–169 (2005).
15. Falk, F., and Kanopka, P., "Three-dimensional Landau theory describing the martensitic phase transformation of shape-memory alloys," *J. Phys.: Condens. Matter* **2**, 61–77 (1990).
16. Levitas, V. I., and Preston, D. L., "Three-dimensional Landau theory for multivariant stress-induced martensitic phase transformations. I. Austenite $\leftrightarrow$ martensite," *Phys. Rev. B* **66**, 134206 (2002).
17. Levitas, V. I., and Preston, D. L., "Three-dimensional Landau theory for multivariant stress-induced martensitic phase transformations. II. Multivariant phase transformations and stress space analysis," *Phys. Rev. B*, **66**, 134207 (2002).
18. Levitas, V. I., Preston, D. L., and Lee, D. W., "Three-dimensional Landau theory for multivariant stress-induced martensitic phase transformations. III. Alternative potentials, critical nuclei, kink solutions, and dislocation theory," *Phys. Rev. B* **68**, 134201 (2003).
19. Mahapatra, D. R., and Melnik, R. V. N., "A dynamic model for phase transformations in 3D samples of shape memory alloys," *Lect. Notes Compu. Sci.* Springer-Verlag, **3516**, 25–32 (2005).
20. Wu, X., Grummon, D. S., and Pence, T. J., "Modeling phase fraction shakedown during thermomechanical cycling of shape memory materials," *Mater. Sci. Engng. A* **273–275**, 245–250 (1999).
21. Roy Mahapatra, D., and Melnik, R. V. N., "Finite element approach to modelling evolution of 3D shape memory materials," *Math. Computers Simul.* (in press) July 2006.
22. Li, B., and Luskin, M., "Finite element analysis of microstructure for the cubic to tetragonal transformation," *SIAM J. Numer. Anal.* **35**, 376–392 (1998).
23. Matus, P., Melnik, R. V. N., Wang, L., and Rybak, I., "Application of fully conservative schemes in nonlinear thermoelasticity: modelling shape memory materials," *Math. Computers Simul.* **65**, 489–510 (2004).
24. Fu, S., Huo, S. Y., and Muller, I., "Thermodynamics of pseudoelasticity—an analytical approach," *Acta Mechanica* **99**, 1–19 (1991).
25. Simo, J. C., and Hughes, T. J. R., Computational Inelasticity, Springer-Verlag (1997).